Journal of Power Sources 196 (2011) 9708–9718

Contents lists available at ScienceDirect

Journal of Power Sources

journal homepage: www.elsevier.com/locate/jpowsour

Physics-based lithium ion silver vanadium oxide cathode model

Derek A. Strange[a], Sean Rayman[a], Jesse S. Shaffer[b], Ralph E. White[c,*]

[a] Department of Chemical Engineering, University of South Carolina, Columbia, SC 29208, USA
[b] Shaffer Consulting LLC, 301 Spartan Drive, Columbia, SC 29212, USA
[c] 209 Edgemont Street, Easley, SC 29642, USA

ARTICLE INFO

Article history:
Received 15 June 2011
Accepted 15 July 2011
Available online 22 July 2011

Keywords:
Lithium primary battery
SVO
Cathode
Mathematical model
Redlich–Kister

ABSTRACT

A cathode half cell physics-based model for a St. Jude Medical fabricated silver vanadium oxide (SVO) cathode coin cell battery was constructed. The model is based on a single particle Fick's second law approach with the open-circuit potential modeled with a Redlich–Kister equation. By assuming that lithium ions intercalate only through the ends of the cuboid SVO particles, the model is able to predict accurately the discharge profile of experimental cathode half cell coin cells.

1. Introduction

Lithium ion silver vanadium oxide (Li-SVO) intercalation electrode batteries are one of the most commonly used cells for modern implantable cardiac defibrillator devices. The SVO reduction reaction observed during discharge has been characterized by Gomadam et al. [1] as

$$(x_G + y_G)Li^+ + (x_G + y_G)e^- + Ag_2{}^{+}V_4{}^{5+}O_{11} \rightarrow Li_{x_G+y_G}{}^{+}Ag_{2-x_G}{}^{+}V_{y_G}{}^{4+}V_{4-y_G}{}^{5+}O_{11} + x_G Ag^0$$

where x_G goes from zero to two and y_G goes from zero to four. Gomadam et al. claim this reaction can be treated mathematically as a combination of two parallel reactions [1].

$$x_G Li^+ + x_G e^- + Ag_2{}^{+}V_4{}^{5+}O_{11} \rightarrow Li_{x_G}{}^{+}Ag_{2-x_G}{}^{+}V_4{}^{5+}O_{11} + x_G Ag^0$$

$$y_G Li^+ + y_G e^- + Ag_2{}^{+}V_4{}^{5+}O_{11} \rightarrow Li_{y_G}{}^{+}Ag_2{}^{+}V_{y_G}{}^{4+}V_{4-y_G}{}^{5+}O_{11}$$

The SVO model developed by Gomadam et al. [1] provided an approach to modeling of Li-SVO cathodes by using Butler–Volmer equations to govern electrode kinetics for each reaction and then linking the reaction current density to the depth of discharge (DoD) through Faraday's law. They made the following assumptions,

1. The cathode limits battery capacity, such that there is excess Li in the anode.
2. The cathode dominates battery resistance and contributions to the resistance from the anode and separator are negligible.
3. The cathode is kinetically limited, meaning the ohmic and mass transfer resistances are negligible, such that the reaction current is uniform throughout the porous electrode.
4. The effects of heat generation, degradation, and parasitic reactions are negligible.
5. The SVO particles are cylindrical in shape.

Their model was limited by a purely empirical fit of the open-circuit potential (OCP) as a function of DoD while also not addressing potential diffusion limitations from mass transfer resistance. Also, they indicated that in their hybrid SVO-CF_x cathode system, their assumption of negligible ohmic resistance was valid up until a particular value of a reaction current distribution parameter, determined by a ratio of the effective ohmic resistance to the applied current density and based on the cathode design parameters. A later paper by Gomadam et al. [2] then expanded their earlier model to include ohmic resistance effects. The paper in [2] does not mention any considerations for mass transfer limitations, however. If the assumption in [1] of no mass transfer resistances is perpetuated in [2], the basis for their limits of applicability may be incorrect.

In this work, a proprietary form of SVO developed by St. Jude Medical (SJM) with a one reaction system is used:

$$7Li^+ + 7e^- + Ag_2V_4{}^{5+}O_{11} \rightarrow Li_7{}^{+}V_2{}^{4+}V_2{}^{3+}O_{11} + 2Ag^0$$

* Corresponding author. Tel.: +1 803 777 3270.
E-mail address: white@cec.sc.edu (R.E. White).

0378-7753/$ – see front matter © 2011 Elsevier B.V. All rights reserved.
doi:10.1016/j.jpowsour.2011.07.057

Nomenclature

A_k	Redlich–Kister coefficient (J mol^{-1})
A_p	particle electrochemically active surface area (cm^2)
C	dimensionless lithium ion concentration
c_{Li}	lithium ion concentration (mol cm^{-3})
$c_{Li,0}$	initial lithium ion concentration (mol cm^{-3})
c_e	electrolyte phase lithium ion concentration (mol cm^{-3})
$c_{Li,j,max}$	maximum intercalatable lithium ion concentration (mol cm^{-3})
$c_{Li,j,avg}$	average lithium ion concentration (mol cm^{-3})
$c_{Li,j,surf}$	surface lithium ion concentration (mol cm^{-3})
D_{Li}	concentration-dependent diffusion coefficient of lithium ions into SVO (cm^2 s^{-1})
E	electrode potential (V)
F	Faraday's constant (96,485 C mol^{-1} e$^-$)
G_E	excess Gibbs free energy (J)
H	particle half-height (cm)
I_{app}	applied current (A)
i_j	current density for electrode j (A cm^{-2})
i_0	exchange current density (A cm^{-2})
j	positive (p) or negative (n) electrode
k_j	rate constant (cm$^{2.5}$ mol$^{-0.5}$ s^{-1})
K	rate terms in Eqs. (23)–(25)
L	particle length from center to one end (cm)
M	number of terms in Redlich–Kister expansion
m_a	active mass of SVO (g)
M_{SV}	SVO molecular weight (g mol^{-1})
N	number of nodes in method of lines
$\underline{N_{Li}}$	net flux density of lithium ions into the particle (mol Li$^+$ cm^{-2} s^{-1})
n_e	number of electrons transferred during total reaction
R_g	ideal gas constant (8.314 J mol^{-1} K^{-1})
R_{Li}	rate of reaction (mol Li$^+$ cm^{-3} s^{-1})
R_{ohm}	ohmic resistance (Ω)
s_{Li}	lithium ion stoichiometric coefficient for total reaction
S_{EA}	electroactive surface area (cm^2)
T	temperature (K)
T_{ref}	reference temperature (K)
t	time (s)
t_+	initial time (s)
U_n	SVO open-circuit potential (V)
U_n^0	standard SVO open-circuit potential (V)
u_{Li}	mobility of Li$^+$ (mol Li$^+$ cm^2 J^{-1} s^{-1})
V_a	volume active material (cm^3)
V_e	electrode volume (cm^3)
V_p	particle electrochemically active volume (cm^3)
$\underline{v}$	velocity of the bulk fluid (cm s^{-1})
W	particle half-width (cm)
$x_{Li,n,surf}$	surface depth of discharge as defined by Eq. (19) for the negative electrode
$x_{Li,n,avg}$	average depth of discharge as defined by Eq. (26) for the negative electrode
Z	dimensionless distance from center of particle
z_{Li}	charge number of the reactive species
$\alpha_{a,j}$	anodic transfer coefficient for electrode j
$\alpha_{c,j}$	cathodic transfer coefficient for electrode j
β_j	symmetry coefficient
ρ	bulk SVO density (g cm^{-3})
τ	dimensionless time
η_j	overpotential of electrode j (V)
ε	cathode fraction active material
$\gamma_{Li,n,surf}$	activity coefficient of intercalated lithium
φ_1	solid-phase potential (V)
φ_2	electrolyte-phase potential (V)
θ_{Li}	inflection terms in Eqs. (23)–(25)

This paper extends the Gomadam et al. model by using the single particle framework to model the transport within the particle, allowing for solid phase mass transfer limitations. The ohmic resistance is also included on an order of magnitude basis from experimental SJM data, rather than assuming a negligible ohmic resistance within a range of applicability. In order to reduce the dependence on empirical fits, the model presented here uses the Redlich–Kister (R–K) equation to fit the open-circuit profile rather than an empirical fit as performed by Gomadam et al.

Atlung et al. [3] presented a single particle (SP) model for an intercalation electrode. They described a system of intercalation electrodes using an electrolyte salt of the anode material and an organic solvent. In such a system, cation transport was affected by diffusion and migration effects, where the diffusion effects dominated in the solid phase. Cell behavior was then controlled by the electrolyte–electrode interface concentrations of the ion. With this in mind, Atlung et al. attempted to model the discharge profile of intercalation electrode batteries based on the cathode particles and their geometry. They assumed that the cation and electron fluxes were uniform over the entire particle surface and that all cathode particles were in contact with a current collector matrix. Under these assumptions, they based their modeling on a single particle of the cathode material [3].

The work done by Atlung et al. served as a basis for the SP modeling approach. Haran et al. [4] expanded on the work by Atlung et al. by proposing a general system of equations for solving lithium intercalation into a SP intercalation electrode. The work done by Haran et al. included work by Paxton and Newman [5] to solve for the diffusion coefficient in such a system, but such work is not applied in this paper due to the presence of plateaus in the OCP of Li-SVO that Paxton and Newman claimed may influence their method. This paper also does not address resistive elements expanded on in work by Zhang et al. [6] or the analytical solution for diffusion applied by Guo et al. [7].

Several assumptions are made here when using the SP approach. As presented by Santhanagopalan et al. [8],

1. The concentration of lithium ions in the electrolyte is large and independent of position and time.
2. The ionic conductivity of the electrolyte is sufficient enough and the flux of ions small enough that there is no potential drop in the solution phase.
3. The electronic conductivity of the porous electrodes is large enough and the current small enough such that there is no electronic potential gradient in the electrodes.
4. All the cathode particles are uniformly distributed throughout the cathode and are of the same geometry.

Assumptions 1–4 guarantee that the difference in the potential of the electrolyte and active material is independent of position. Thus, the flux of lithium ions into each particle is independent of the particle's position. Therefore, a large number of the same size particles with the same current density at the surface of the particle can be used to represent the entire cathode. Also assumed for this work:

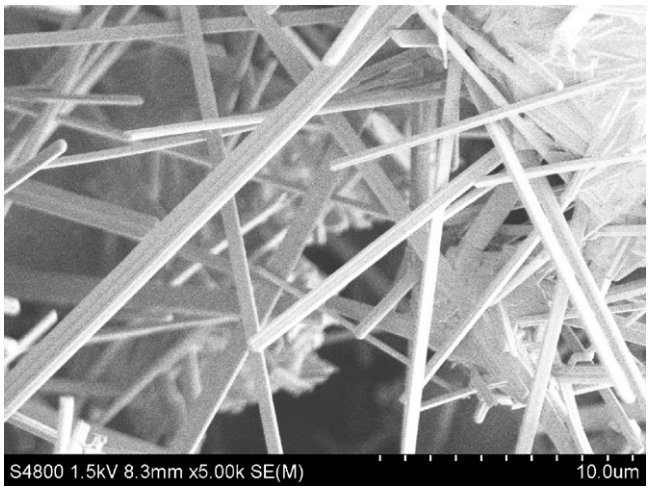

Fig. 1. SEM image of pure SVO crystals displaying cuboid geometry.

5. That the oxidation of lithium metal in the anode occurs close to the OCP of the Li/Li$^+$ reaction and that there is a large excess of lithium metal in the anode compared to the amount of lithium that can be intercalated into the cathode.

The main advantage of applying the SP method over other concentration-based frameworks is the SP method provides a simpler system of equations while giving accurate results for the $C/100$ (253 μA) current load that will be examined in this work. The more significant improvement is in using a concentration-based framework instead of using Faraday's law to link the reaction current density and DoD as done in the work by Gomadam et al. Through the concentration-based framework, one can include mass transfer resistance limitations through diffusion into the particle, not addressed by Gomadam et al. This offers insight into how the concentration of Li$^+$ varies inside the particle. In future work, this can be expanded to account for relaxation from pulse effects during pulse discharge.

2. Modeling

2.1. Mode of intercalation

A SEM image of SJM SVO particles, Fig. 1, indicates that the particles are cuboid in shape instead of the assumption in work by Gomadam et al. [1] that SVO particles were cylindrical in geometry. An idealized geometry of the SJM SVO particle is shown in Fig. 2 and has a length of $2L$, a height of $2H$, and a width of $2W$. SEM images taken by Chen et al. [9] also show that along the length of these particles there are strata. The particles themselves have been described as "tunnel-like" [10]. The work of Chen et al., combined with observations drawn from work by Takeuchi et al. [11], supports the hypothesis that lithium ions intercalate into the ends of the particle along the length of these strata. However, the diffusion length from the end caps to the center of the particle is significantly larger than from the sides of the particle to the center, which may allow lithium ions to diffuse through the sides of the particle as well.

Thus, two limiting cases are raised, one case where intercalation only happens from the ends of the particle and one case where intercalation only happens from the sides of the particle. Mechanical processes used by SJM to grind SVO material down to smaller particle sizes are often rated by their ability to affect particle length, with total particle length varying from a few microns up to 100 μm. Particle width and height also generally do not vary

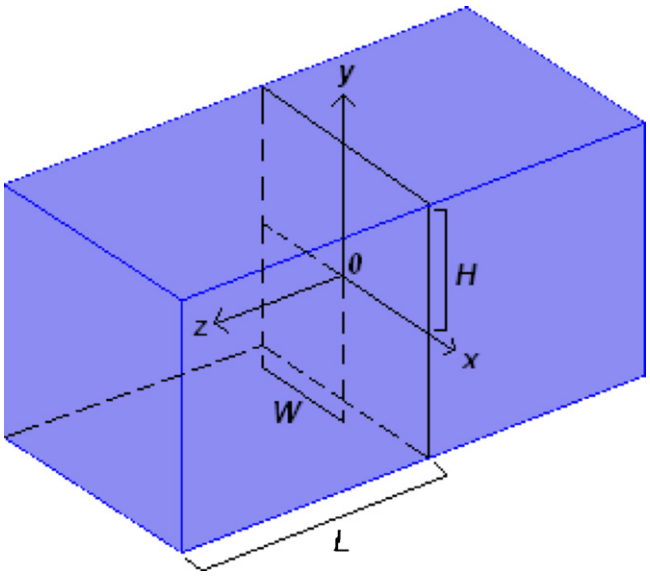

Fig. 2. Example SVO particle, figure not drawn to scale.

by significant margins, typically only a few microns in size and are unaffected by the grinding process. As such, in the interest of determining the effect of mechanical processing on discharge behavior, this work will concern itself with the limiting case where intercalation only happens from the ends of the particle. Specifically, the particle will be modeled such that Li$^+$ intercalates from one end to the center of the particle. The particle will therefore be treated as a one-dimensional slab as seen in the simple line drawing in Fig. 3.

2.2. Fick's second law

The material balance for a particle is described by Eqs. (1) and (2).

$$\frac{\partial c_{Li}}{\partial t} = -\nabla \cdot \underline{N}_{Li} + R_{Li} \tag{1}$$

$$\underline{N}_{Li} = -z_{Li} u_{Li} F c_{Li} \nabla \phi_1 - D_{Li}(c_{Li}) \nabla c_{Li} + c_{Li} \underline{v} \tag{2}$$

where $\underline{N}_{Li}$ is the net flux density of lithium ions into the particle (mol Li$^+$ cm^{-2} s^{-1}), c_{Li} is the lithium ion concentration in the particle (mol Li$^+$ cm^{-3}), R_{Li} is the rate of reaction (mol Li$^+$ cm^{-3} s^{-1}), z_{Li} is the charge number of the reactive species, u_{Li} is the mobility of Li$^+$ (mol Li$^+$ cm^2 J^{-1} s^{-1}), φ_1 is the solid-phase potential (J), D_{Li} is the diffusion coefficient of lithium ions in the SVO particle (cm^2 s^{-1}) as a function of lithium ion concentration, and $\underline{v}$ is the velocity of the bulk fluid (cm s^{-1}). Because this is a solid phase, $\underline{v} = 0$, and due to assumption 3, $\nabla\phi_1 = 0$. Also, since the reaction takes place at the surface of the particle, $R_{Li} = 0$. This reduces the material balance to Eq. (3), Fick's second law.

$$\frac{\partial c_{Li}}{\partial t} = -\nabla \cdot (-D_{Li}(c_{Li}) \nabla c_{Li}) = D_{Li}(c_{Li}) \left(\frac{\partial^2 c_{Li}}{\partial x^2} + \frac{\partial^2 c_{Li}}{\partial y^2} + \frac{\partial^2 c_{Li}}{\partial z^2} \right) + [\nabla \cdot D_{Li}(c_{Li})] \nabla c_{Li} \tag{3}$$

Eq. (3) can be simplified by assuming that diffusion occurs only along the direction of the z-axis, the slab approximation.

$$\frac{\partial c_{Li}}{\partial t} = D_{Li}(c_{Li}) \cdot \frac{\partial^2 c_{Li}}{\partial z^2} + \frac{\partial D_{Li}(c_{Li})}{\partial c_{Li} \cdot (\partial c_{Li}/\partial z)^2} \tag{4}$$

At some initial time, t_+, the concentration of lithium ions is some initial value, $c_{Li,0}$, due to some prior discharge to test for possible cell failure before beginning normal discharge of the cell. The initial

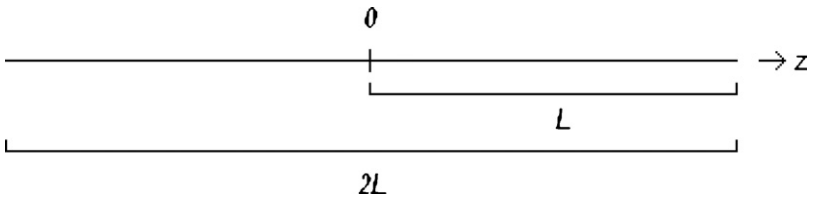

Fig. 3. Line drawing of SVO particle studied. Intercalation from one end to center only.

concentration is left as an adjustable parameter to be estimated using nonlinear least squares.

$$c_{\mathrm{Li}}(z, t = t_+) = c_{\mathrm{Li},0} \tag{5}$$

Because symmetry was assumed there is no flux of lithium ions at $z = 0$, the center of the slab [12].

$$\frac{\partial c_{\mathrm{Li}}}{\partial z}(0, t) = 0 \tag{6}$$

At the surface of the particle, $z = L$, the flux of lithium ions into the particle is proportional to the current density:

$$\frac{\partial c_{\mathrm{Li}}}{\partial z}(L, t) = -\frac{s_{\mathrm{Li}} I_{app}}{n_e F D_{\mathrm{Li}}(c_{\mathrm{Li}}) S_{EA}} \tag{7}$$

where I_{app} is the applied current (A), n_e is the number of electrons transferred during the total reaction, s_{Li} is the stoichiometric coefficient of Li^+ in the overall reaction which is taken to be seven in this paper ($s_{\mathrm{Li}} = 7$), F is Faraday's constant (96485 C mol^{-1} e$^-$), and S_{EA} is the electroactive surface area of the particle (cm^2).

The electroactive surface area, S_{EA}, is defined as the electrochemically active surface area of material within the electrode, or the volume of active material within the electrode ($\varepsilon_e V_e$) multiplied by the ratio of electrochemically active surface area of the particle to particle volume (A_p/V_p) [7].

$$S_{EA} = \frac{A_p \varepsilon_e V_e}{V_p} \tag{8}$$

where A_p is the active surface area of the particle, V_p is the volume of the particle, V_e is the volume of the electrode, and ε_e is the volume fraction of active material. The volume fraction of active material is defined as the volume of active material within the electrode divided by the total volume within the electrode. If the mass of active material and the bulk density of the material are known, the volume of active material, V_a, can be determined via Eq. (9).

$$V_a = \frac{m_a}{\rho} \tag{9}$$

Eq. (10) defines the volume fraction of active material.

$$\varepsilon_e = \frac{V_a}{V_e} \tag{10}$$

Depending on particle geometry, the surface area to volume ratio will change. For slab geometry, where the particle is treated as a one-dimensional entity by assuming lithium only intercalates through the ends of the particle, and examining the slab from its center to one end only, Eq. (11) applies.

$$A_p = 2(2H \cdot 2W) \quad V_p = 2L \cdot 2W \cdot 2H \quad \frac{A_p}{V_p} = \frac{1}{L} \tag{11}$$

Substituting Eqs. (9)–(11) into Eq. (8) expresses the electroactive surface area as Eq. (12).

$$S_{EA} = \frac{m_a}{L\rho} \tag{12}$$

Another way of expressing this equation is that the electroactive surface area is the mass of active SVO material multiplied by the electroactive specific surface area of the section of the particle under examination. If one were to assume lithium ions intercalated into the SVO particle from all directions, the electroactive surface area to volume ratio would become the specific surface area of the entire particle. Since the endcap intercalation limiting case is being investigated in this paper, only the specific surface area of the ends of the particle is utilized in the present model.

The boundary conditions defined by Eqs. (6) and (7) with the previously defined governing equation, Eq. (4), and initial condition, Eq. (5), provide the basis for determining lithium ion concentration within the particle as a function of time and distance. In order to increase the level of confidence in modeling results, the present model is implemented in two different programs, COMSOL Multiphysics and MATLAB. COMSOL allows for a more automated solution of systems of equations, whereas MATLAB gives greater freedom in programming of solution steps. In order to allow for changes in geometric properties in COMSOL without having to reconstruct the particle geometry, the governing equation, initial condition, and boundary conditions can be expressed in dimensionless terms by introducing the dimensionless variables in Eq. (13) [12].

$$C = \frac{c_{\mathrm{Li}}}{c_{\mathrm{Li},0}} - 1 \quad Z = \frac{v}{L} \quad \tau = \frac{D_{\mathrm{Li}}(c_{\mathrm{Li}})t}{L^2} \tag{13}$$

Applying these variables to the governing equation, initial condition, and boundary conditions gives Eqs. (14)–(17).

$$C(Z, \tau = \tau_+) = 0 \tag{14}$$

$$\frac{\partial C}{\partial \tau} = \frac{\partial^2 C}{\partial Z^2} + \frac{1}{D_{\mathrm{Li}}(c_{\mathrm{Li}})} \frac{\partial D_{\mathrm{Li}}}{\partial C} \left(\frac{\partial C}{\partial Z} \right)^2 \tag{15}$$

$$\frac{\partial C}{\partial Z}(0, \tau) = 0 \tag{16}$$

$$\frac{\partial C}{\partial Z}(1, \tau) = -\frac{s_{\mathrm{Li}} I_{app} L}{n_e F D_{\mathrm{Li}}(c_{\mathrm{Li}}) S_{EA} c_{\mathrm{Li},0}} \tag{17}$$

These equations can then be placed into COMSOL Multiphysics to solve for the dimensionless concentration as a function of dimensionless distance and dimensionless time after specifying the applied current, I_{app}, initial concentration, $c_{\mathrm{Li},0}$, and all other parameters.

2.3. Reaction kinetics

The generalized electrochemical reactions for intercalation and deintercalation at a solid/solution phase interface as described by Guo et al. [7] are written as

$$\mathrm{Li} - \theta_S \overset{\text{Deintercalation}}{\longrightarrow} \mathrm{Li}^+ + \mathrm{e}^- + \theta_S$$

$$\mathrm{Li} - \theta_S \underset{\text{Intercalation}}{\longleftarrow} \mathrm{Li}^+ + \mathrm{e}^- + \theta_S$$

where Li–θ_S is an intercalation site filled by a lithium ion and θ_S represents an unfilled intercalation site [7]. The rate of these reactions can then be solved with Eq. (18), the Butler–Volmer equation (Appendix A), based on the DoD at the surface of the particle, $x_{\mathrm{Li},j,surf}$,

defined by Eq. (19) and the electrode overpotential, η_j, defined by Eq. (20) and neglecting the electrolyte potential.

$$i_j = k_j F c_{\mathrm{Li},j,\max} c_e^{0.5} x_{\mathrm{Li},j,surf}^{0.5} (1 - x_{\mathrm{Li},j,surf})^{0.5} \times \left\{ \exp\left[\frac{0.5F}{R_g T}\eta_j\right] - \exp\left[-\frac{0.5F}{R_g T}\eta_j\right] \right\} \quad (18)$$

$$x_{\mathrm{Li},j,surf} = \frac{c_{\mathrm{Li},j,surf}}{c_{\mathrm{Li},j,\max}} \qquad c_{\mathrm{Li},n,\max} = \frac{s_{\mathrm{Li}}\rho}{M_{SV}} \quad (19)$$

$$\eta_j = E_j - U_j \quad (20)$$

where subscript j refers to the positive (p) or negative (n) electrode, i_j is the current density ($\mathrm{A\,cm^{-2}}$), k_j is the rate constant ($\mathrm{cm^{2.5}\,mol^{-1}\,s^{-1}}$), $c_{Li,j,max}$ is the maximum concentration of lithium ions that can be intercalated into the particle ($\mathrm{mol\,cm^{-3}}$), c_e is the concentration of lithium ions in the electrolyte phase ($\mathrm{1E{-}03\,mol\,cm^{-3}}$), ρ is the bulk density of SVO ($\mathrm{4.789\,g\,cm^{-3}}$ [1]), M_{SV} is the molecular weight of SVO ($\mathrm{595.5\,g\,mol^{-1}}$), E_j is the electrode potential (V), and U_j is the OCP (V) referenced to a $\mathrm{Li/Li^+}$ reference electrode. Because a $\mathrm{Li/Li^+}$ reference electrode is used for U_j, the anode is lithium metal, and the current used is so small, the anode potential is assumed to be negligible. Thus, the cathode potential plus the ohmic resistance is the cell potential and anodic terms are neglected. Including the dimensionless variables from Eq. (13) and the ohmic resistance, Eq. (18) can be rewritten as Eq. (21).

$$E_n = I_{app}R_{ohm} + U_n + \frac{R_g T}{0.5F} a\sinh \times \left\{ \frac{2I_{app}}{S_{EA}Fk_n c_e^{0.5}[c_{\mathrm{Li},0}(C(1,\tau)+1)]^{0.5}[c_{\mathrm{Li},n,\max} - c_{\mathrm{Li},0}(C(1,\tau)+1)]^{0.5}} \right\} \quad (21)$$

where $C(1,\tau)$ is the dimensionless concentration at the surface of the particle and $x_{\mathrm{Li},n,surf} = c_{\mathrm{Li},0}(C(1,\tau)+1)/c_{\mathrm{Li},n,\max}$.

2.4. Open-circuit potential modeling

The OCP of Li-SVO changes over the course of DoD such that without an accurate model of the OCP, the discharge profile cannot be properly modeled. The way in which the OCP changes with DoD at the surface of the particle, however, is a property of how the material was fabricated, requiring fitting of an OCP model to experimental data. In literature, a purely empirical fit to the data is sometimes used, such as in work by Gomadam et al. [1]. The fit in [1] is peculiar in that it splits the OCP data curve into two separate curves, each modeled with different equations that are designed to be run simultaneously. The resulting OCP curve from the two equations working together, however, does not match up identically with the source data.

In order to minimize the level of empirical analysis and match more closely with available OCP data, another way of fitting the OCP is used in this work. Karthikeyan et al. [13] showed that the OCP of a lithium intercalation electrode can be accurately modeled using the R–K equation to estimate the excess Gibbs free energy (Appendix B). The resulting OCP equation when used in Eq. (21) is given by Eq. (22), where DoD is defined by Eq. (19) as the Butler–Volmer equation is only valid at the surface of the particle [13].

$$FU_n = FU_n^0 + R_g T_{ref} \ln\left(\frac{1 - x_{\mathrm{Li},n,surf}}{x_{\mathrm{Li},n,surf}}\right) + \left\{ \sum_{k=0}^{M} A_k \cdot \times \left[(2x_{\mathrm{Li},n,surf} - 1)^{k+1} - \frac{2x_{\mathrm{Li},n,surf} k (1 - x_{\mathrm{Li},n,surf})}{(2x_{\mathrm{Li},n,surf} - 1)^{1-k}} \right] \right\} \quad (22)$$

The advantage of using the R–K fit over a purely empirical fit is the R–K equation provides physical insight for why the OCP curve changes over the DoD, relating the OCP behavior to electrochemical phenomena. Fig. 4 gives a comparison of the OCP of the SJM cell under study where the non-idealities due to activity are ignored, reducing the equation to the classical Nernst equation, and where the non-idealities are accounted for in the full R–K equation. Work done by Colclasure and Kee [14] demonstrate how the R–K method could be expanded to estimate the activity coefficient and then applied that to determine the exchange current density.

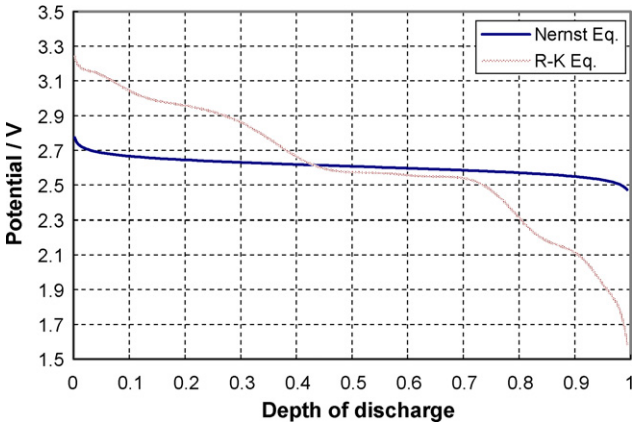

Fig. 4. Comparison of the open-circuit potential modeled where non-idealities from activity are ignored (Nernst equation) and accounted for (R–K equation).

2.5. Parameter estimation

The R–K coefficients A_k and U_n^0 are considered unknown parameters in the model. Since SVO is sensitive to the manner in which it is produced, the open-circuit profile is distinct for each method of preparation. Fig. 5 is provided as an example of how the OCP profile for SVO can differ widely based on the manner in which the material was produced [1,15]. In order to allow the R–K equation to model the OCP based on input data from a desired formulation of SVO, the R–K coefficients are considered adjustable parameters and determined by performing a nonlinear least squares fit to experimental OCP data using MATLAB and the MATLAB routine LSQNONLIN.

Focusing on fitting the first 70% DoD, one can observe from Fig. 6 that there is a difference between OCP and experimental discharge data that is larger in the first 40% of discharge in comparison to subsequent regions. This has been reported previously within literature and attributed by Crespi and West to temporary insertion of lithium ions into an alternative set of sites due to the slow rate of

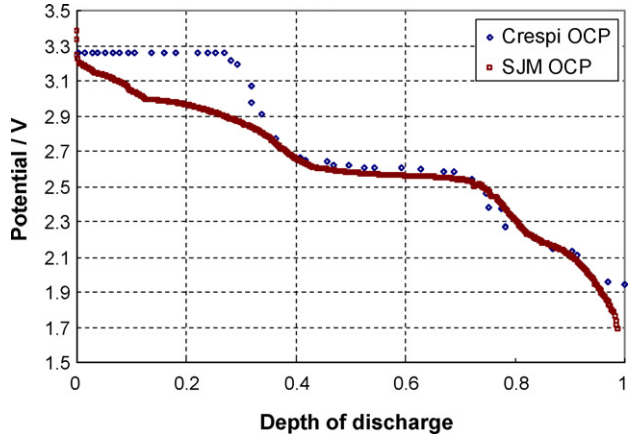

Fig. 5. Comparison of OCP profiles from SVO manufactured by SJM and Crespi et al. [1,15].

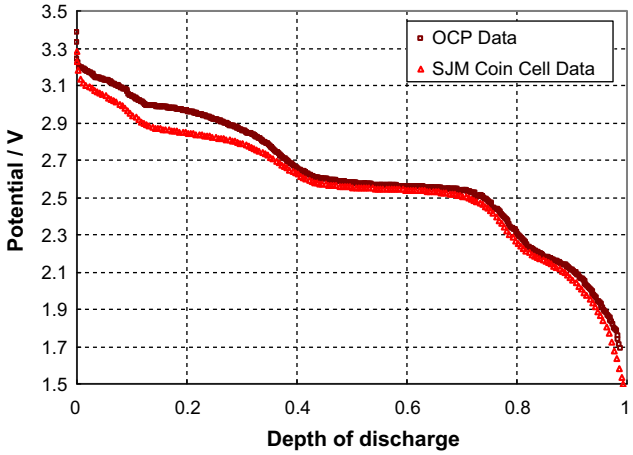

Fig. 6. Raw SJM OCP and $C/100$ (253 μA) SJM coin cell discharge data.

the thermodynamically preferred reaction [16]. In this paper, the greater difference between OCP and experimental cell potential in the first 40% DoD compared to the rest of discharge is used as an aid in fitting the diffusion coefficient, D_{Li}, and rate constant, k_n. The rate constant is allowed to vary over the extent of discharge. The justification behind this is the reduction of silver to silver metal appears to have a significant effect on cell performance, also noted in work by Gomadam et al. [1]. Eq. (23) is used to vary the rate constant for this work and was derived based on best apparent fit to the discharge data.

$$k_n(c_{\mathrm{Li}}) = k_{n,1} + \frac{k_{n,2} - k_{n,1}}{1 + \exp[-K_1((c_{\mathrm{Li},n,surf}/c_{\mathrm{Li},n,\max}) - \theta_{\mathrm{Li},1})]} + \frac{k_{n,3} - k_{n,2}}{1 + \exp[-K_2((c_{\mathrm{Li},n,surf}/c_{\mathrm{Li},n,\max}) - \theta_{\mathrm{Li},2})]} \quad (23)$$

where the K terms define how quickly the equation changes between values and the θ_{Li} terms refer to the inflection points in the resulting curve. Similarly, the diffusion coefficient D_{Li} has been shown in literature to vary over the course of discharge. Data for fitting the diffusion coefficient, however, are insufficient within the literature. Results from Ramasamy et al. [17] show a diffusion coefficient that monotonically decreases with DoD. Results from Takeuchi et al. [18], however, report a diffusion coefficient that experiences irregular spikes and dips as discharge proceeds. The irregular behavior of the diffusion coefficient during discharge is also supported by results from Lee and Popov [19]. One should note that the results obtained by the Ramasamy, Takeuchi, and Lee groups do not agree. This would imply a strong dependence on the specific mix of SVO used. Since literature sources are inconsistent and there are insufficient experimental diffusion coefficient data available to develop a detailed equation for the SVO mix of interest, an empirical equation is used. Eq. (24) is a function of Li^+ concentration in the particle and was developed along with Eq. (23) from best apparent fit to discharge data.

$$D_{\mathrm{Li}}(c_{\mathrm{Li}}) = D_{\mathrm{Li},1} + \frac{D_{\mathrm{Li},2} - D_{\mathrm{Li},1}}{1 + \exp[-K_3((c_{\mathrm{Li}}(z)/c_{\mathrm{Li},n,\max}) - \theta_{\mathrm{Li},3})]} + \frac{D_{\mathrm{Li},3} - D_{\mathrm{Li},2}}{1 + \exp[-K_4((c_{\mathrm{Li}}(z)/c_{\mathrm{Li},n,\max}) - \theta_{\mathrm{Li},4})]} \quad (24)$$

MATLAB and LSQNONLIN can be used to fit the parameters to the data with a nonlinear least squares fit. The rate constant, diffusion coefficient, and initial concentration were fitted simultaneously. Eqs. (4)–(7) were solved using the method of lines with 50 node points in MATLAB (Appendix C) and the finite element technique in COMSOL.

Table 1
Modeling constants.

Parameter	Units	Value
$c_{\mathrm{Li},n,max}$	mol Li^+ cm^{-3}	5.629E−02
c_e	mol Li^+ cm^{-3}	1E−03
I_{app}	A	−253E−06
L	cm	25E−04
m_a	g	0.0803
M	–	15
M_{SV}	g mol^{-1}	595.5
N	–	50
n_e	mol e^- mol^{-1} SVO	7
S_{EA}	cm^2	6.707
T	K	310.15
T_{ref}	K	310.15
β_j	–	0.5
ρ	g cm^{-3}	4.789
s_{Li}	mol Li^+ mol^{-1} SVO	7

The assumption is made in work by Gomadam et al. that the effect of ohmic resistance is negligible at low current loads. In this work, the ohmic resistance is included and allowed to vary over depth of discharge through Eq. (25). Since resistance data were unavailable for the fitted coin cell, using Eq. (25) with the parameters defined in Table 3 allows for an ohmic resistance on the order of magnitude seen in similar SJM SVO coin cells. Additionally, all values of K and θ_{Li} used in Eqs. (23)–(25) were set arbitrarily to roughly represent observed reaction steps in work by Leising et al. [10].

$$R_{ohm}(c_{\mathrm{Li}}) = R_{ohm,1} + \frac{R_{ohm,2} - R_{ohm,1}}{1 + \exp[-K_5((c_{\mathrm{Li},n,surf}/c_{\mathrm{Li},n,\max}) - \theta_{\mathrm{Li},5})]} + \frac{R_{ohm,3} - R_{ohm,2}}{1 + \exp[-K_6((c_{\mathrm{Li},n,surf}/c_{\mathrm{Li},n,\max}) - \theta_{\mathrm{Li},6})]} \quad (25)$$

3. Results

The model developed in this work was applied to a coin cell described in Table 1 with experimental discharge data shown in Fig. 6. The OCP of the cell is independent of any changes to SVO mass or particle length and is modeled using MATLAB to fit the R–K expansion out to seventeen terms, including U_n^0 and A_0. The resulting fit is plotted in Fig. 7 and the R–K coefficient values tabulated in Table 2. The fit extrapolates to the final reported DoD the coin cell was modeled to. Part of the attractiveness in using the R–K equation

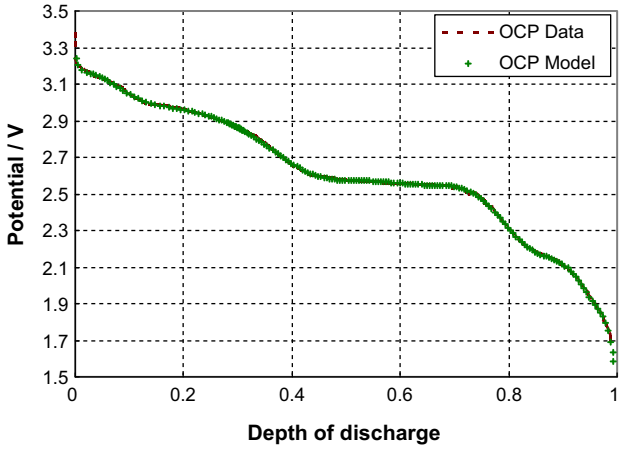

Fig. 7. Modeled OCP compared to experimental SJM OCP data.

Table 2
Redlich–Kister coefficients for SJM SVO determined through parameter estimation. U_n^0 is in V and the R–K coefficient terms are in units J mol^{-1}.

Parameter	Value
U_n^0	2.608
A_0	−4.576E+04
A_1	6.621E+03
A_2	−4.578E+04
A_3	−4.700E+04
A_4	3.298E+05
A_5	−1.872E+05
A_6	−2.034E+06
A_7	5.935E+05
A_8	6.575E+06
A_9	5.883E+05
A_{10}	−1.097E+07
A_{11}	−3.529E+06
A_{12}	8.993E+06
A_{13}	4.067E+06
A_{14}	−2.877E+06
A_{15}	−1.521E+06

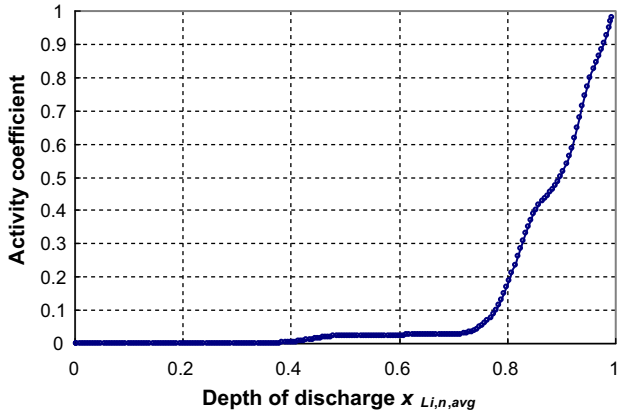

Fig. 8. Activity coefficient determined using estimated Redlich–Kister parameters.

is that it can be related back to the activity coefficient (Appendix B) [13,14]. The activity coefficient is plotted versus average particle DoD, defined by Eq. (26), in Fig. 8.

$$x_{\mathrm{Li},n,avg} = \frac{c_{\mathrm{Li},n,avg}}{c_{\mathrm{Li},n,\max}} \tag{26}$$

In work done by Leising et al. [10], the claim is made that electrochemical activity of a Li-SVO cell is dominated by reduction of silver to silver metal, which lasts until around 34% DoD. This is represented in Fig. 8 as a very low activity coefficient, meaning there is a very strong tendency for Li^+ to intercalate into SVO. In the region from 34% to 54% DoD, Leising et al. claims the electrochemical activity switches to a purely V^{5+} to V^{4+} reduction, reflected as a higher activity coefficient in Fig. 8. After 54% DoD, Leising et al. states there is a competition between reducing V^{5+} to V^{4+} and V^{4+} to V^{3+}. The OCP drops gradually in this region up until around 74% DoD, when a more dramatic drop in potential begins to occur, leading to the conclusion that the V^{4+} to V^{3+} reduction becomes dominant at this point. In Fig. 8, the activity coefficient also rapidly begins to approach unity after around 74% DoD. Thus, the activity coefficient is demonstrating the sudden drop in useful capacity beyond 74% DoD as lithium ions become more difficult to intercalate into SVO. These results provide a basis for using the 74% DoD mark as an end of life indicator for the cell, which is also used by SJM.

Both MATLAB and COMSOL can now be used to show the concentration and discharge profiles with both time and position within the particle. First consider the previously described coin cell under constant discharge. MATLAB is used to perform parameter estimation and fit the model to the experimental data. The resulting fit is shown in Fig. 9, where DoD is based on Eq. (26), with parameter values in Table 3. The modeled fit very closely matches the experimental data except for the region from 5% to 10% DoD. The discrepancy between the model predictions and the experimental data is attributed to inaccuracies in how the rate constant, plotted in Fig. 10, and diffusion coefficient, plotted in Fig. 11 on a log scale, are determined. Fig. 12 plots the diffusion coefficient calculated from Eq. (24) on a log scale versus cell potential and compares those results to results reported by Lee and Popov [19]. One should note that the SVO used in the work by Lee and Popov may be considerably different from the SJM SVO studied in this paper, and also approaches the diffusivity from an electrode basis rather than a single particle that has been limited to intercalation from one end only. From the comparison, a conclusion could be drawn that the diffusion coefficient as calculated by Eq. (24) should start at a value several orders of magnitude higher and then decrease as the DoD approaches 10%. Increasing the complexity of the empirical equations utilized is expected to resolve the discrepancy. Fig. 13 shows how the concentration within the particle varies across the length of the particle at a single point in time. This leads to the conclusion that on the chosen current load, the concentration across the

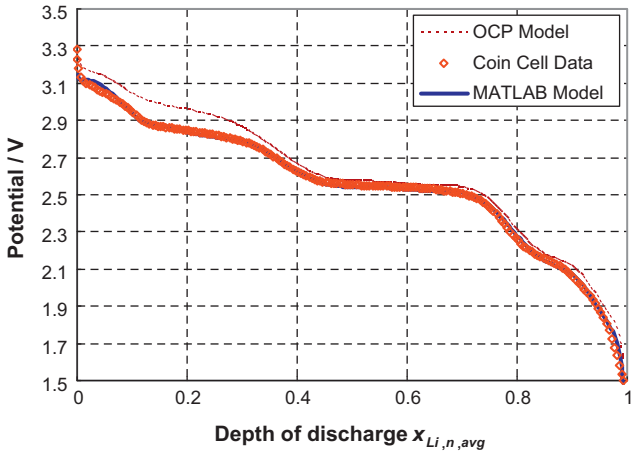

Fig. 9. Fitted MATLAB model compared to SJM OCP data and $C/100$ (253 μA) SJM coin cell data.

Table 3
Estimated discharge fitting parameters for SJM discharge data.

Parameter	Units	Value
$c_{\mathrm{Li},0}$	mol Li^+ cm^{-3}	7.506E−05
$k_{n,1}$	cm$^{2.5}$ mol$^{-0.5}$ s^{-1}	3.781E−06
$k_{n,2}$	cm$^{2.5}$ mol$^{-0.5}$ s^{-1}	2.662E−07
$k_{n,3}$	cm$^{2.5}$ mol$^{-0.5}$ s^{-1}	1.873E−06
$D_{\mathrm{Li},1}$	cm^2 s^{-1}	3.897E−10
$D_{\mathrm{Li},2}$	cm^2 s^{-1}	7.969E−11
$D_{\mathrm{Li},3}$	cm^2 s^{-1}	2.570E−08
$R_{ohm,1}$	Ω	13.07
$R_{ohm,2}$	Ω	10.07
$R_{ohm,3}$	Ω	7.063
K_1	–	50
K_2	–	10
K_3	–	50
K_4	–	100
K_5	–	100
K_6	–	30
$\theta_{\mathrm{Li},1}$	–	0.100
$\theta_{\mathrm{Li},2}$	–	0.380
$\theta_{\mathrm{Li},3}$	–	0.090
$\theta_{\mathrm{Li},4}$	–	0.340
$\theta_{\mathrm{Li},5}$	–	0.150
$\theta_{\mathrm{Li},6}$	–	0.300

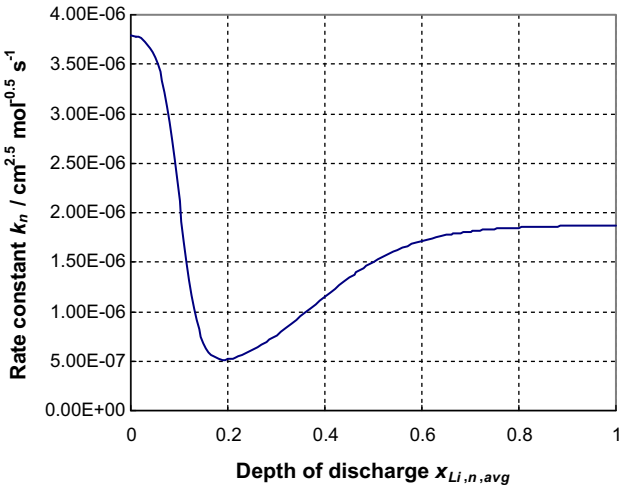

Fig. 10. Rate constant varying with discharge based on Eq. (23) and estimated parameters.

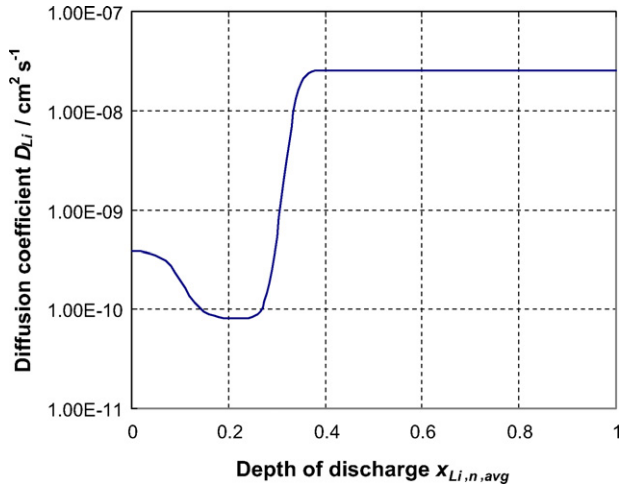

Fig. 11. Diffusion coefficient varying with discharge based on Eq. (24) and estimated parameters.

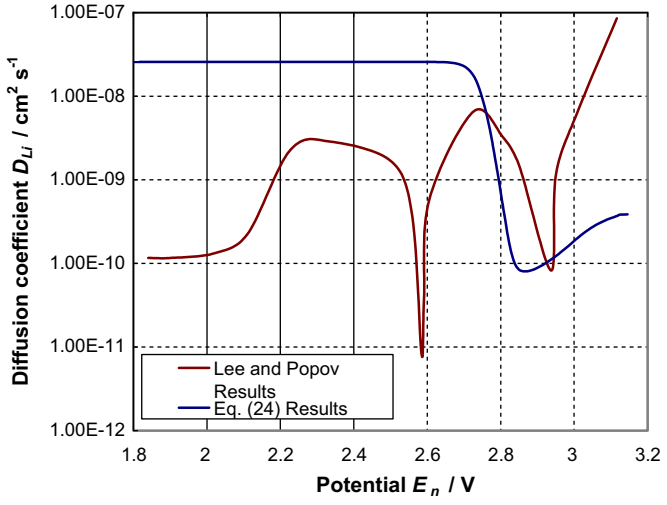

Fig. 12. Diffusion coefficient as calculated from Eq. (24) compared to results from Lee and Popov [19].

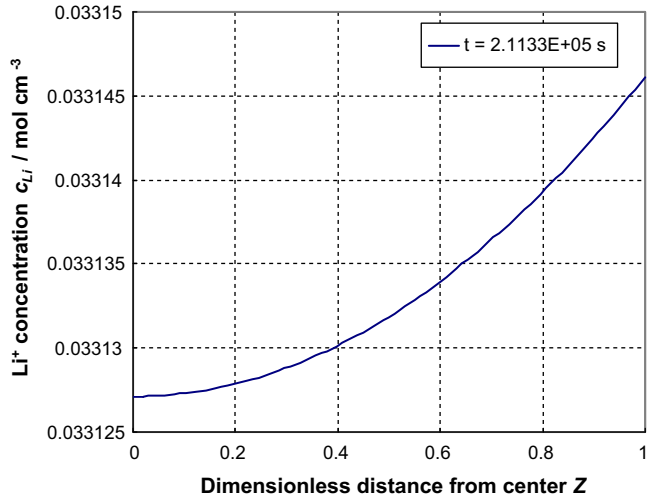

Fig. 13. Concentration profile in a $C/100$ (253 μA) coin cell particle with changing distance from center.

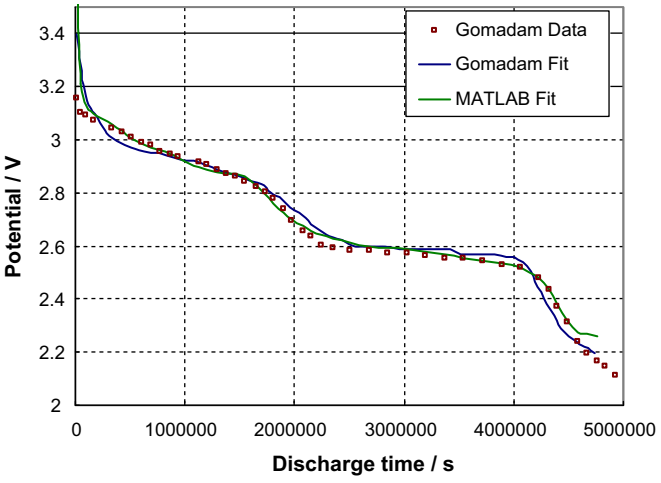

Fig. 14. Comparison between Gomadam et al. and MATLAB fits to Gomadam et al. 1000 μA discharge data [1].

length of the particle could be considered constant. Even at the low 253 μA current load chosen, however, the effect of the concentration gradient across the particle on the discharge profile and estimated parameter values was determined to be significant.

In order to be confident in the validity of the numerical results, the MATLAB model results were also compared against results generated by COMSOL Multiphysics, which numerically solves for Fick's second law using a finite element technique. Using parameter values estimated with MATLAB in the COMSOL model, the cell potential vs. DoD results were compared to determine the error between the two programs. The comparison indicated the two models differed by 0.05% at most. Having established confidence in the model reporting nearly identical results in two solution programs, the model is compared versus the Gomadam et al. model [1] to determine if the new model more accurately fits experimental data. Fig. 14 plots cell potential versus time for the 1000 μA experimental discharge data used by Gomadam et al., the fit they achieved to the data, and the fit achieved with the new model using parameter values in Tables 4, 5 and 6 . The data for the Gomadam et al. fit was taken directly from their plot as the fit given in their paper was unable to be replicated by the authors of this paper. The new model appears to fit accurately the Gomadam et al. discharge data better than or at least as well as the model reported in their work.

Table 4
Modeling constants for Gomadam et al. [1] cell.

Parameter	Units	Value
$c_{Li,n,max}$	mol Li^+ cm^{-3}	4.825E−02
c_e	mol Li^+ cm^{-3}	1E−03
I_{app}	A	−1000E−06
L	cm	5E−05
m_a	g	5.109
M	–	15
M_{SV}	g mol^{-1}	595.5
N	–	50
n_e	mol e^- mol^{-1} SVO	6
S_{EA}	cm^2	2.134E+04
T	K	310.15
T_{ref}	K	310.15
β_j	–	0.5
ρ	g cm^{-3}	4.789
s_{Li}	mol Li^+ mol^{-1} SVO	6

Table 5
Redlich–Kister coefficients for Gomadam et al. [1] SVO determined through parameter estimation. U_n^0 is in V and the R–K coefficient terms are in units J mol^{-1}.

Parameter	Value
U_n^0	2.902
A_0	−2.908E+04
A_1	7.992E+03
A_2	4.055E+04
A_3	−1.039E+05
A_4	−1.930E+05
A_5	7.446E+05
A_6	3.898E+05
A_7	−2.998E+06
A_8	1.267E+05
A_9	6.887E+06
A_{10}	−1.912E+06
A_{11}	−9.024E+06
A_{12}	2.726E+06
A_{13}	6.244E+06
A_{14}	−1.203E+06
A_{15}	−1.733E+06

Table 6
Estimated discharge fitting parameters for Gomadam et al. [1] 1000 μA discharge data.

Parameter	Units	Value
$c_{Li,0}$	mol Li^+ cm^{-3}	3.749E−06
$k_{n,1}$	$cm^{2.5}$ $mol^{-0.5}$ s^{-1}	2.081E−09
$k_{n,2}$	$cm^{2.5}$ $mol^{-0.5}$ s^{-1}	9.164E−11
$k_{n,3}$	$cm^{2.5}$ $mol^{-0.5}$ s^{-1}	9.418E−11
$D_{Li,1}$	cm^2 s^{-1}	7.600E−15
$D_{Li,2}$	cm^2 s^{-1}	1.405E−15
$D_{Li,3}$	cm^2 s^{-1}	5.158E−15
$R_{ohm,1}$	Ω	13.07
$R_{ohm,2}$	Ω	10.07
$R_{ohm,3}$	Ω	7.063
K_1	–	30
K_2	–	150
K_3	–	100
K_4	–	20
K_5	–	100
K_6	–	30
$\theta_{Li,1}$	–	0.100
$\theta_{Li,2}$	–	0.340
$\theta_{Li,3}$	–	0.300
$\theta_{Li,4}$	–	0.540
$\theta_{Li,5}$	–	0.150
$\theta_{Li,6}$	–	0.300

A final point of interest is the effect of mechanical processing of the SVO material on the discharge profile. This was done for the studied coin cell by altering the diffusion length of the particle, L, with results plotted in Fig. 15. Smaller particle sizes improve performance of the cell, but also of note is that particle length affects discharge behavior in the first 40% of discharge. Were the length of the particle to change during discharge, accounting for how the length changes could play a significant role in modeling. A distribution of particle sizes might also exist as opposed to the present model which assumes all particles have the same size.

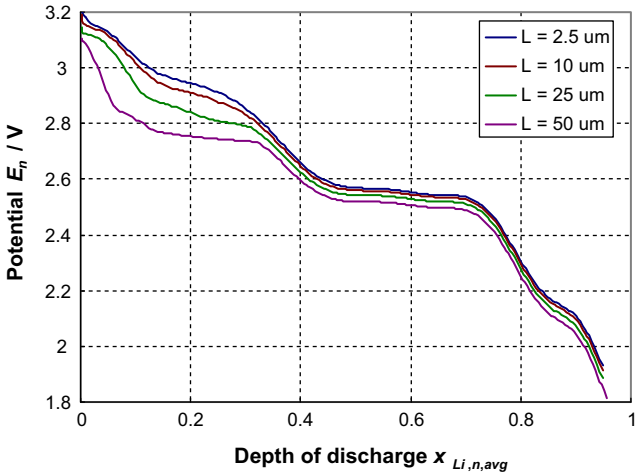

Fig. 15. Effect of particle diffusion length on discharge profile at $C/100$ (253 μA) discharge.

4. Conclusions

Using the R–K equation an excellent fit to experimental OCP data from SJM Li-SVO cells was obtained, eliminating the need to use empirical equations to model the OCP. Use of the R–K equation is supported by activity results consistent with literature sources and industry standards. The single particle model using Fick's second law can be used to determine cell parameters ($k_{n,1}$, $D_{Li,1}$, $D_{Li,2}$, etc.) and also predict cell behavior during discharge.

5. Future work

As previously mentioned, the method of determining the diffusion coefficient requires further refinement. Examination of discharge behavior on a different path of intercalation (i.e. from the sides) was also considered, but was not done in this paper. While there is evidence to support the limiting case where lithium ions intercalate only through the ends of the particle, no absolute determination has been made. Examining the particle assuming a limiting case where lithium intercalates only through the sides of the particle or relaxing the limits and letting lithium intercalate from all directions into the particle may allow for constructing a more accurate model.

Acknowledgements

The authors would like to thank St. Jude Medical for supplied financial support and experimental data. SEM work done at the St. Jude Medical plant in Liberty, South Carolina.

Appendix A.

The generalized electrochemical reactions for intercalation and deintercalation at a solid/solution phase interface as described by Guo et al. [7] are written as

$$Li - \theta_S \overset{\text{Deintercalation}}{\longrightarrow} Li^+ + e^- + \theta_S$$

$$\mathrm{Li} - \theta_S \underset{\text{Intercalation}}{\longleftarrow} \mathrm{Li}^+ + \mathrm{e}^- + \theta_S$$

where Li–θ_S is an intercalation site filled by a lithium ion and θ_S represents an unfilled intercalation site [7]. The concentration of filled sites on the surface of the particle is the same as the concentration of lithium ions on the surface, giving Eq. (A.1).

$$c_{\mathrm{Li}-\theta_S} = c_{\mathrm{Li},j}\big|_{z=L} = x_{\mathrm{Li},j,surf}\, c_{\mathrm{Li},j,\max} \tag{A.1}$$

Here, subscript j refers to the positive (p) or negative (n) electrode. The concentration of unfilled sites is then described by Eq. (A.2).

$$c_{\theta_S} = c_{\mathrm{Li},j,\max} - c_{\mathrm{Li},j}\big|_{z=L} = (1 - x_{\mathrm{Li},j,surf})c_{\mathrm{Li},j,\max} \tag{A.2}$$

Taking into account the first assumption made for the SP approach, the electrolyte lithium ion concentration, c_e, is also kept constant at 1E−03 mol Li^+ cm^{-3} [7].

The current density for the deintercalation and intercalation reactions can then be described by Eqs. (A.3) and (A.4), assuming a negligible electrolyte potential.

$$\vec{i}_j = \vec{k}_j \frac{n_e}{s_{\mathrm{Li}}} F c_{\mathrm{Li},j,\max} x_{\mathrm{Li},j,surf} \exp\left[\frac{\alpha_{a,j}F}{R_g T}(\phi_{1,j} - \phi_{2,j})\right] \tag{A.3}$$

$$\overleftarrow{i}_j = \overleftarrow{k}_j \frac{n_e}{s_{\mathrm{Li}}} F c_{\mathrm{Li},j,\max} c_e (1 - x_{\mathrm{Li},j,surf}) \exp\left[-\frac{\alpha_{c,j}F}{R_g T}(\phi_{1,j} - \phi_{2,j})\right] \tag{A.4}$$

where the k_j terms are the deintercalation ($\rightarrow$) and intercalation ($\leftarrow$) rate constants for electrode j, respectively; $\alpha_{a,j}$ is the anodic transfer coefficient for the deintercalation reaction at electrode j; and $\alpha_{c,j}$ is the cathodic transfer coefficient for the intercalation reaction at electrode j. An exchange current density can also be described as the reaction current density at open-circuit conditions, or when $\varphi_{1,j} - \varphi_{2,j} = U_j$.

$$i_{0,j,1} = \vec{k}_j \frac{n_e}{s_{\mathrm{Li}}} F c_{\mathrm{Li},j,\max} x_{\mathrm{Li},j,surf} \exp\left[\frac{\alpha_{a,j}F}{R_g T} U_j\right] \tag{A.5}$$

$$i_{0,j,2} = \overleftarrow{k}_j \frac{n_e}{s_{\mathrm{Li}}} F c_{\mathrm{Li},j,\max} c_e (1 - x_{\mathrm{Li},j,surf}) \exp\left[-\frac{\alpha_{c,j}F}{R_g T} U_j\right] \tag{A.6}$$

$$i_{0,j,1} = i_{0,j,2} = i_{0,j} \tag{A.7}$$

If one assumes $\alpha_{a,j} + \alpha_{c,j} = 1$, the exponential terms in Eqs. (A.5) and (A.6) can be removed by raising Eq. (A.5) to the $\alpha_{c,j}$, raising Eq. (A.6) to the $\alpha_{a,j}$, and multiplying the two together. If the condition in Eq. (A.7) is also taken into account, Eq. (A.8) is formed.

$$i_{0,j} = (i_{0,j,1})^{\alpha_{c,j}} (i_{0,j,2})^{\alpha_{a,j}} = \vec{k}_j^{\alpha_{c,j}} \overleftarrow{k}_j^{\alpha_{a,j}} \frac{n_e}{s_{\mathrm{Li}}} F c_{\mathrm{Li},j,\max} c_e^{\alpha_{a,j}} x_{\mathrm{Li},j,surf}^{\alpha_{c,j}} \times (1 - x_{\mathrm{Li},j,surf})^{\alpha_{a,j}} \exp\left[\frac{\alpha_{a,j}\alpha_{c,j}}{R_g T} U_j\right] \exp\left[\frac{-\alpha_{a,j}\alpha_{c,j}}{R_g T} U_j\right] \tag{A.8}$$

The exchange current density can then be rewritten as Eq. (A.9), assuming the rate constant $k_j = \vec{k}_j^{\alpha_{c,j}} \overleftarrow{k}_j^{\alpha_{a,j}}$ [7].

$$i_{0,j} = k_j \frac{n_e}{s_{\mathrm{Li}}} F c_{\mathrm{Li},j,\max} c_e^{\alpha_{a,j}} x_{\mathrm{Li},j,surf}^{\alpha_{c,j}} (1 - x_{\mathrm{Li},j,surf})^{\alpha_{a,j}} \tag{A.9}$$

The current density equations can be rewritten in terms of the exchange current density.

$$\vec{i}_j = i_{0,j} \exp\left[\frac{\alpha_{a,j}F}{R_g T}(\phi_{1,j} - \phi_{2,j} - U_j)\right] \tag{A.10}$$

$$\overleftarrow{i}_j = -i_{0,j} \exp\left[-\frac{\alpha_{c,j}F}{R_g T}(\phi_{1,j} - \phi_{2,j} - U_j)\right] \tag{A.11}$$

The electrode overpotential, or drop from open-circuit conditions due to losses, is described as:

$$\eta_j = \phi_{1,j} - \phi_{2,j} - U_j \tag{A.12}$$

Eq. (A.12) can then be substituted back into Eqs. (A.10) and (A.11). The net current produced by the intercalation/deintercalation reaction is therefore:

$$\begin{aligned} i_j = \vec{i}_j + \overleftarrow{i}_j &= i_{0,j}\left[\exp\left(\frac{\alpha_{a,j}F}{R_g T}\eta_j\right) - \exp\left(-\frac{\alpha_{c,j}F}{R_g T}\eta_j\right)\right] \\ &= k_j \frac{n_e}{s_{\mathrm{Li}}} F c_{\mathrm{Li},j,\max} c_e^{\alpha_{a,j}} x_{\mathrm{Li},j,surf}^{\alpha_{c,j}} (1 - x_{\mathrm{Li},j,surf})^{\alpha_{a,j}} \\ &\times \left[\exp\left(\frac{\alpha_{a,j}F}{R_g T}\eta_j\right) - \exp\left(-\frac{\alpha_{c,j}F}{R_g T}\eta_j\right)\right] \end{aligned} \tag{A.13}$$

Eq. (A.13) is also known as the Butler–Volmer equation [7].

For the Li-SVO reaction under consideration and neglecting the electrolyte phase potential, the electrode overpotential is defined by Eq. (A.14).

$$\eta_j = E_j - U_j \tag{A.14}$$

Here, E_j is the electrode potential (V). Because a $\mathrm{Li/Li}^+$ reference electrode is used for U_j, the anode is lithium metal, and the current used is so small, the anode potential is assumed to be negligible. Thus, the cathode potential plus the ohmic resistance term is the cell potential. The anodic and cathodic transfer coefficients are also redefined as the symmetry coefficient, β_j, multiplied by n_e/s_{Li}. With the symmetry coefficient held constant at 0.5 and n_e/s_{Li} held constant at one, Eq. (A.13) becomes Eq. (A.15).

$$i_n = k_n F c_{\mathrm{Li},n,\max}^{0.5} c_e^{0.5} x_{\mathrm{Li},n,surf}^{0.5} (1 - x_{\mathrm{Li},n,surf})^{0.5} \times \left\{ \begin{array}{l} \exp\left[\dfrac{0.5F}{R_g T}(E_n - U_n)\right] \\ -\exp\left[-\dfrac{0.5F}{R_g T}(E_n - U_n)\right] \end{array} \right\} \tag{A.15}$$

The current density is defined through Eq. (A.16) as the applied current divided by the electroactive surface area.

$$i_n = \frac{I_{app}}{S_{EA}} \tag{A.16}$$

Eq. (A.15) can be rewritten as Eq. (A.17).

$$E_n = I_{app} R_{ohm} + U_n + \frac{R_g T}{0.5F} a\sinh \times \left\{ \frac{2I_{app}}{S_{EA} F k_n c_e^{0.5} [c_{\mathrm{Li},0}(C(1,\tau)+1)]^{0.5} [c_{\mathrm{Li},n,\max} - c_{\mathrm{Li},0}(C(1,\tau)+1)]^{0.5}} \right\} \tag{A.17}$$

Appendix B.

An examination of electrochemical potentials allows for an alternative method for estimating the OCP of lithium intercalation electrodes, though in-depth analyses of these potentials are beyond the scope of this work. The method replicated here was developed by Karthikeyan et al. [13], restricted in scope in this paper to estimating the OCP. First, the intercalation electrode equilibrium potential relative to a lithium reference electrode can be represented by Eq. (B.1), where α refers to the intercalated species and β refers to vacant sites [13].

$$\frac{n_e}{s_{\mathrm{Li}}} F U_n = \mu_{\mathrm{Li}}^0 + \mu_\beta - \mu_\alpha \tag{B.1}$$

Here, the electrochemical potential μ_i of species i can be expressed in terms of an activity coefficient, mole fraction, and reference electrochemical potential via Eq. (B.2).

$$\mu_i = \mu_i^0 + R_g T \ln(\gamma_i x_i) \tag{B.2}$$

where subscript i refers to α or β. Eq. (B.2) can be substituted into Eq. (B.1) resulting in Eq. (B.3), which can be used to represent the OCP profile.

$$\frac{n_e}{s_{\mathrm{Li}}} FU_n = \mu_{\mathrm{Li}}^0 + \mu_\beta^0 - \mu_\alpha^0 + R_g T \ln\left(\frac{x_\beta}{x_\alpha}\right) + R_g T \ln\left(\frac{\gamma_\beta}{\gamma_\alpha}\right)$$
$$= \frac{n_e}{s_{\mathrm{Li}}} FU_n^0 + R_g T \ln\left(\frac{x_\beta}{x_\alpha}\right) + R_g T \ln\left(\frac{\gamma_\beta}{\gamma_\alpha}\right) \tag{B.3}$$

If unit activity is assumed, Eq. (B.3) reduces to the classic Nernst equation, Eq. (B.4) [13].

$$\frac{n_e}{s_{\mathrm{Li}}} FU_n = \frac{n_e}{s_{\mathrm{Li}}} FU_n^0 + R_g T \ln\left(\frac{x_\beta}{x_\alpha}\right) \tag{B.4}$$

If unit activity is not assumed, the activity coefficients can be related back to the partial molar excess Gibbs free energy through Eq. (B.5).

$$R_g T \ln(\gamma_i) = \overline{g}_i^E = \frac{\partial}{\partial n_i}(n_t G_E)_{T,P,l\neq i} \tag{B.5}$$

Here, subscript l refers to α or β. The R–K equation can then be used to approximate the excess Gibbs free energy [13].

$$G_E = x_{\alpha,n} x_{\beta,n} \sum_{k=0}^{M} A_k (x_{\alpha,n} - x_{\beta,n})^k$$
$$= x_{\alpha,n}(1 - x_{\alpha,n}) \sum_{k=0}^{M} A_k (2x_{\alpha,n} - 1)^k \tag{B.6}$$

Eq. (B.6) can be substituted back into Eqs. (B.3) and (B.5) to obtain Eq. (B.7). Eq. (B.7) is the form used in Eq. (21) for the OCP.

$$\frac{n_e}{s_{\mathrm{Li}}} FU_n = \frac{n_e}{s_{\mathrm{Li}}} FU_n^0 + R_g T_{ref} \ln\left(\frac{1 - x_{\mathrm{Li},n,surf}}{x_{\mathrm{Li},n,surf}}\right)$$
$$+ \left\{ \sum_{k=0}^{M} A_k \cdot \left[(2x_{\mathrm{Li},n,surf} - 1)^{k+1} - \frac{2x_{\mathrm{Li},n,surf} k (1 - x_{\mathrm{Li},n,surf})}{(2x_{\mathrm{Li},n,surf} - 1)^{1-k}} \right] \right\} \tag{B.7}$$

One can also solve for the activity coefficient of the intercalated material via Eq. (B.8) [13].

$$R_g T \ln(\gamma_{\mathrm{Li},n,surf}) = \sum_{k=0}^{M} A_k (1 - x_{\mathrm{Li},n,surf})^2 (2x_{\mathrm{Li},n,surf} - 1)^k$$
$$\times \left[\frac{2x_{\mathrm{Li},n,surf} k}{(2x_{\mathrm{Li},n,surf} - 1)} + 1 \right] \tag{B.8}$$

Appendix C.

The treatment of the governing equation, Eq. (4), and boundary conditions, Eqs. (6) and (7), while utilizing MATLAB deserves mention, as MATLAB does not automatically solve for Fick's second law whereas COMSOL does. Instead, Fick's second law is broken apart from a partial differential equation into a series of ordinary differential equations using the method of lines approach. This divides the particle along its length into individual nodes, calculating the concentration at each point. For the modeling performed in this work, $N = 50$ nodes are used. Defining the center of the particle as the first node, $m = 1$, and the surface of the particle as the last node, $m = N = 50$, Eq. (C.1) solves for the central nodes.

$$\frac{dc_{\mathrm{Li},n,m}}{dt} = D_{\mathrm{Li}} \frac{(c_{\mathrm{Li},n,m-1} - 2c_{\mathrm{Li},n,m} + c_{\mathrm{Li},n,m+1})}{(L/(N-1))^2} \quad m = 2, N-1 \tag{C.1}$$

where $L/(N-1)$ breaks the particle into equal-length segments and L is the half-length of the particle (cm). The boundary conditions at the center of the particle, Eq. (C.2), and at the surface, Eq. (C.3), are also included, using forwards and backwards finite difference techniques, respectively.

$$D_{\mathrm{Li}}(c_{\mathrm{Li},n,1}) \frac{dc_{\mathrm{Li},n,1}}{dz} = D_{\mathrm{Li}}(c_{\mathrm{Li},n,1}) \frac{3c_{\mathrm{Li},n,1} - 4c_{\mathrm{Li},n,2} + c_{\mathrm{Li},n,3}}{2(L/(N-1))} = 0 \tag{C.2}$$

$$D_{\mathrm{Li}}(c_{\mathrm{Li},n,N}) \frac{dc_{\mathrm{Li},n,N}}{dz} = - D_{\mathrm{Li}}(c_{\mathrm{Li},n,N}) \frac{3c_{\mathrm{Li},n,N} - 4c_{\mathrm{Li},n,N-1} + c_{\mathrm{Li},n,N-2}}{2(L/(N-1))}$$
$$- \frac{I_{app} s_{\mathrm{Li}}}{n_e F S_{EA}} = 0 \tag{C.3}$$

References

[1] P.M. Gomadam, D.R. Merritt, E.R. Scott, C.L. Schmidt, P.M. Skarstad, J.W. Weidner, J. Electrochem. Soc. 154 (11) (2007) A1058–A1064.
[2] P.M. Gomadam, D.R. Merritt, E.R. Scott, C.L. Schmidt, J.W. Weidner, Electrochem. Soc. Trans. 11 (30) (2008) 1–6.
[3] S. Atlung, K. West, T. Jacobsen, J. Electrochem. Soc. 126 (8) (1979) 1311–1321.
[4] B.S. Haran, B.N. Popov, R.E. White, J. Electrochem. Soc. 145 (12) (1998) 4082–4089.
[5] B. Paxton, J. Newman, J. Electrochem. Soc. 143 (4) (1996) 1287–1292.
[6] D. Zhang, B.N. Popov, R.E. White, J. Electrochem. Soc. 147 (3) (2000) 831–838.
[7] M. Guo, G. Sikha, R.E. White, J. Electrochem. Soc. 158 (2) (2011) A122–A132.
[8] S. Santhanagopalan, Q. Guo, P. Ramadass, R.E. White, J. Power Sources 156 (2006) 620–628.
[9] Z. Chen, S. Gao, R. Li, M. Wei, K. Wei, H. Zhou, Electrochim. Acta 53 (2008) 8134–8137.
[10] R.A. Leising, W.C. Thiebolt III, E.S. Takeuchi, Inorg. Chem. 33 (25) (1994) 5733–5740.
[11] K.J. Takeuchi, A.C. Marschilok, S.M. Davis, R.A. Leising, E.S. Takeuchi, Coord. Chem. Rev. 219–221 (2001) 283–310.
[12] V.R. Subramanian, R.E. White, J. Power Sources 96 (2001) 385–395.
[13] D.K. Karthikeyan, G. Sikha, R.E. White, J. Power Sources 185 (2008) 1398–1407.
[14] A.M. Colclasure, R.J. Kee, Electrochim. Acta 55 (2010) 8960–8973.
[15] A.M. Crespi, P.M. Skarstad, H.W. Zandbergen, J. Power Sources 54 (1995) 68–71.
[16] K. West, A.M. Crespi, J. Power Sources 54 (1995) 334–337.
[17] R.P. Ramasamy, C. Feger, T. Strange, B.N. Popov, J. Appl. Electrochem. 36 (2006) 487–497.
[18] E.S. Takeuchi, W.C. Thiebolt III, Electrochem. Soc. Proc. 89 (1989) 72–80.
[19] J.-W. Lee, B.N. Popov, J. Power Sources 161 (2006) 565–572.